A pressure-loss model for flow-through round-hole perforated plates of moderate porosity and thickness in laminar and turbulent flow regimes

N.B. When citing this work, cite the original published paper.

(article starts on next page)

A pressure-loss model for flow-through round-hole perforated plates of moderate porosity and thickness in laminar and turbulent flow regimes

Shuai Li [a,*], Lars Davidson [a], Shia-Hui Peng [a,b]

[a] *Department of Mechanics and Maritime Sciences, Chalmers University of Technology, SE-412 96 Gothenburg, Sweden*
[b] *FOI - Swedish Defense Research Agency, SE-164 90 Stockholm, Sweden*

ARTICLE INFO

ABSTRACT

In this paper, we proposed a novel fluid flow model for pressure loss through plates with circular perforations in both laminar and turbulent flows. The design of this model is based on the recent measurements conducted at ONERA in the framework of the ongoing European Union H2020 INVENTOR project, as well as an existing model for laminar flows. The new model is then validated against existing numerical simulations in the laminar regime and experiments in the turbulent regime. Overall, the predictions given by the new model agree well with the numerical simulations and experiments, and are superior to other models in the literature. This is significant, considering that the present model is much simpler than these previous models. To demonstrate the applicability of the new model in numerical simulations, two-dimensional channel flows are simulated using Reynolds-averaged Navier–Stokes (RANS) equations with the new model as a pressure-drop source term added to the momentum equations. Results show that the RANS predictions agree very well with the present model predictions.

1. Introduction

A fluid flow through a perforated plate is a common problem in a wide variety of practical applications in thermal, mechanical, chemical, civil, nuclear, ocean and aerospace engineering. To enumerate a few, perforated plates are used for the design of heat transfer devices [1–11] and flow conditioning devices [12–18], the control of flames in combustion chambers [19–24] and turbulence [25–28], the reduction of aerodynamic noise [29–32], and so forth. The flow through a perforated plate usually features flow separation near the leading edge of the pores, contraction until the vena contracta is reached, and expansion after the vena contracta. The major pressure losses are induced by the flow expansion process during which considerable energy dissipation takes place [33].

In heat transfer design, flow maldistribution is a major issue degrading the performance of heat transfer devices [17,34–36]. In practice, perforated plates are commonly used to provide a more uniform flow velocity for heat transfer devices. To ensure good flow uniformity, it is required that the perforated plates provide sufficient pressure drops. As such, it is needed to accurately predict the pressure drop across a perforated plate. Another benefit of perforated plates is that they can

enhance turbulence homogeneity, improving system performance too. However, a disadvantage of perforated plates is that they cause drag increases, leading to more energy consumption in the system. It is thus of great significance to study the pressure losses across perforated plates, and to develop empirical models to estimate a priori the pressure losses for a better compromise between flow conditioning and drag increases.

Previous research on pressure losses through perforated plates can primarily be categorized into experimental and numerical studies. Yavuzkurt & Catchen [37] studied experimentally the dependence of pressure loss on air speed with a set of wind-tunnel tests on seven perforated plates of different thicknesses and porosities at different air speeds up to 76 m/s. It was found that, for most of the plates, the pressure loss increases linearly with the square of the air speed, indicating the dominance of inertial pressure losses. For a specific type of plate, small deviations from this linear behaviour can occur, due to a type of wake characterized by large-scale flow oscillations downstream of the plate. Recently, Méry & Sebbane [38] investigated experimentally the pressure loss characteristics of plates with circular perforations of different pore diameters, spacings and plate thicknesses in the framework of the ongoing European Union H2020 INVENTOR project. Fig. 1(a) shows a sketch of a perforated plate with a thickness of δ. The pores
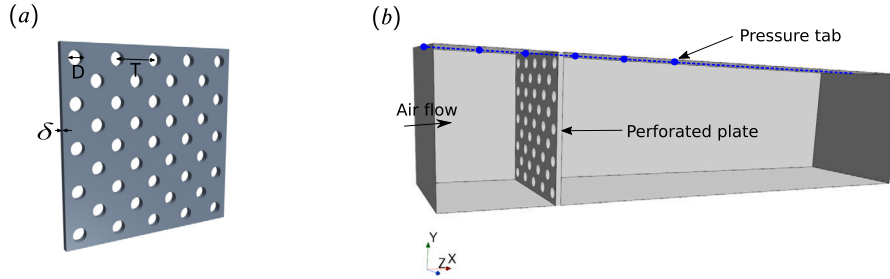
Fig. 1. Sketches of (a) a perforated plate; and (b) the B2A wind-tunnel test section.

have a diameter of D and are separated by a spacing of T. Different pore diameters and spacing of perforated plates lead to different porosity ε which is defined as the ratio between the area of pores and the total area of the perforated plate. It has been shown that the pressure drop coefficient (i.e. pressure drop normalized by the dynamic pressure) is independent of air speed but varies significantly with the plate thickness (δ/D). Through numerical simulations, Bayazit et al. [39] investigated the pressure losses across perforated plates of different thicknesses ($\delta/D = 0.5$ and 1.0) and porosities ($\varepsilon = 0.2$, 0.35 and 0.5) at a wide variety of Reynolds numbers ranging from laminar to turbulent regimes. It was shown that, for laminar flows, higher pressure drops were associated with thicker plates and lower porosities. For turbulent flows, however, the thinner plate caused higher pressure drops as did lower porosities. These trend reversals result from the differences in separated-flow reattachment patterns for the different plate thicknesses in different flow regimes. Bae & Kim [40] numerically studied the pressure losses of laminar flows through thick perforated plates ($\delta/D \geq 1$) at pore-level Reynolds numbers up to 25 and proposed a model, in a mathematically simple form, to predict the pressure loss in laminar regimes. This model was well validated against the experiment but is only applicable to laminar flows. Similarly, based on experiments, a number of models for the pressure loss were proposed by, for example, Idelchik [41], Idelchik [42], Miller [33], Kast [43], Holt et al. [44], ESDU [45] and Malavasi et al. [46], etc. These empirical models are generally applicable to perforated plates of different hole arrangements (i.e. staggered or in-line arrangements) [39,47]. However, these models are much more complicated including parameters to determine using empirical formulae, and are only applicable to high-Reynolds-number turbulent flows. The purpose of the present study is to design a novel model, in a mathematically simple form, but with high predictive accuracies, to characterize the pressure loss through perforated plates in both laminar and turbulent regimes.

In this paper, we construct a correction factor for the Forchheimer coefficient of the Bae & Kim model [40], formulating a new model valid for both laminar and turbulent flow regimes. The correction factor is constructed using the recent experimental data of Méry & Sebbane [38]. The new model is then validated against existing simulation and experimental data in the literature, with comparisons with some other popular

models. Furthermore, to showcase an application of the new model in numerical simulations, we perform two-dimensional channel-flow simulations using RANS with the new model as a pressure-drop source term added to the momentum equations. The RANS-predicted pressure losses are validated against the model-predicted pressure losses, demonstrating the good prediction capabilities of the new model.

The paper is organized as follows: §2 is devoted to a description of the experimental data deployed for the development and validation of the present model for plates with circular perforations. In §3, a discussion of existing perforated-plate models is presented and then a novel model is proposed. In §4, the proposed perforated-plate model is validated against existing numerical simulations in the laminar regime and experiments in the turbulent regime. Then, §5 showcases the application of the proposed model to numerical simulations. Finally, concluding remarks are summarized in §6.

2. The experimental data

In the present study, the experimental data of Méry & Sebbane [38] and Yavuzkurt & Catchen [37] are used to develop and validate, respectively, the novel model for the pressure loss through perforated plates. The measurements were conducted at the Aero-thermo-Acoustics Bench (B2A) of the Office National d'Etudes et de Recherches Aérospatiales (ONERA) and at the Pennsylvania State University, respectively.

The B2A wind tunnel is designed so that the static flow temperature can be accurately regulated from the ambient temperature up to $300\,°C$, with a mean flow bulk Mach number up to 0.5. A 0.2-m-long test section is equipped with two silica windows for optical access. This wind-tunnel cross section has a dimension of 50 mm × 50 mm. A sketch of the wind-tunnel test section is shown in Fig. 1(b). More details on the B2A wind tunnel can be found in Ref. [38,48]. It is important to note that, in this experiment, the perforated plate fully covers the entire cross-section. In other words, the perforated plate has the same dimension as the wind-tunnel cross-section, i.e. 50 mm in width and span. The pressure drop was measured by static pressure taps on the top of the test section upstream and downstream of the perforated plate. Table 1 shows the position of the pressure tabs (PS1 is set as the reference) [38]. The perforated plates are placed in the middle between PS3 and

Table 1
Streamwise position of the pressure tabs.

Pressure tabs	PS1	PS2	PS3	PS4	PS5	PS6	PS7
Streamwise position (mm)	0	15	30	45	60	75	215

Table 2
Parameters of the perforated plates used in the experiment of Méry & Sebbane [38].

Plate	D (mm)	T (mm)	δ (mm)	ε	δ/D
1	5.0	6.0	1.0	0.623	0.20
2	4.0	6.0	1.0	0.403	0.25
3	2.0	3.0	2.0	0.403	1.00
4	2.0	3.0	1.0	0.403	0.50

Table 3
Parameters of the perforated plates used in the experiment of Yavuzkurt & Catchen [37].

Plate	D (mm)	T (mm)	δ (mm)	ε	δ/D
1	1.60	3.18	1.02	0.227	0.638
2	1.91	2.54	0.81	0.510	0.424
3	2.38	6.88	0.91	0.109	0.382
4	2.78	4.76	0.81	0.309	0.291
5	3.18	4.76	0.91	0.403	0.286
6	4.76	9.53	0.97	0.227	0.204
7	3.18	4.76	3.18	0.403	1.000

PS4, namely, 37.5 mm downstream of the PS1 pressure tap. The static pressures are monitored and acquired by a SVMtec differential pressure scanner. A total of 200 samples are acquired with a sampling rate of 10 Hz. The absolute static pressure of the reference pressure tap PS1 is also measured by a 45 Psi Digiquartz absolute pressure sensor in order to provide the absolute static pressure upstream of the perforated plates. For the measurement of the absolute static pressure, a total of 80 samples are acquired with a sampling rate of 4 Hz [38]. In the experiments, the airflow speeds at the wind-tunnel entrance are $U_0 = 16.6$, 25 and 35 m/s, respectively. The experiments are conducted at the ambient temperature (20 °C). These measurements were recently conducted in the framework of the ongoing European Union H2020 INVENTOR project.

The measurements of Yavuzkurt & Catchen [37] were conducted in a pipe-flow apparatus instead of a channel-flow wind tunnel. The internal diameter of the pipe is 90.17 mm. The airflow was provided by a 5 hp blower operated in the suction mode and was controlled using a bypass and an inline valve respectively. The pressure taps were placed 710 mm upstream and downstream from the plate to reduce the effects of local turbulence occurring near the perforated plate. The anemometer used to measure the airflow speed was placed near the upstream opening of the entrance pipe, which provided a relatively uniform distribution of flow velocities across the inlet area of the pipe. The pressure losses were measured over a range from 0 Pa to 3500 Pa. More details on the experimental apparatus can be found in Ref. [37].

Table 2 shows the pore size D, pore spacing T, plate thickness δ and porosity ε of the four perforated plates deployed in the B2A wind-tunnel experiments [38]. The porosity, defined as the ratio between the area of pores and the total area of the perforated plate, can be calculated using the pore size and the pore spacing. Similarly, Table 3 shows the parameters of the seven perforated plates in the experiments of Yavuzkurt & Catchen [37]. The pressure losses measured in Méry & Sebbane [38] and Yavuzkurt & Catchen [37] will be plotted in the following Section 3 and Section 4.

3. Empirical models for pressure loss through perforated plates

The pressure losses caused by flow-through perforated plates are often characterized by the Darcy-Forchheimer equation, as follows

$$-\nabla P = \frac{\mu}{K}U_0 + \rho\alpha|U_0|U_0, \tag{1}$$

where K is the permeability of the porous medium, α is the Forchheimer coefficient or non-Darcy coefficient, ρ is the fluid density, U_0 is the velocity of the incoming flow at the wind-tunnel inlet, and μ is the dynamic viscosity of the fluid. The Darcy term, i.e. the first term on the right-hand side (RHS) of Eq. (1), corresponds to the viscous pressure loss while the Forchheimer term, i.e. the second term on the RHS of Eq. (1), represents the inertial pressure loss. For cases where the pore-level Reynolds number is sufficiently low, the Darcy term strongly dominates over the Forchheimer term [40,47,49,50].

The pressure gradient ($-\nabla P$) on the left-hand side (LHS) of Eq. (1) can also be expressed using the pressure drop (Δp) across the plate with a thickness of δ, as follows

$$-\nabla P = \frac{\Delta p}{\delta}. \tag{2}$$

Then, the Darcy-Forchheimer drag obtained from Eq. (1) can be written as [51]

$$\frac{\Delta p D^2}{\mu \delta U_0} = \frac{D^2}{K} + \varepsilon \alpha D Re_p, \tag{3}$$

where $Re_p = \rho U_0 D/(\mu\varepsilon)$ is the pore-level Reynolds number. From Eq. (3), the normalized pressure drop through perforated plates can be expressed as

$$\frac{\Delta p}{\rho U_0^2} = \frac{\delta D}{K \varepsilon Re_p} + \alpha\delta. \tag{4}$$

The first term on the RHS of Eq. (4) is the contribution of the Darcy term to the normalized pressure drop and depends on both the plate characteristics (permeability, porosities, thickness, etc.) and the flow characteristics (fluid viscosity, flow speed or Reynolds number). The second term in the RHS of Eq. (4) is the Forchheimer contribution and only depends on the plate characteristics (porosities, thickness, etc.).

It is also interesting to note that, for general porous medium, Vafai & Tien [52] included an additional diffusion term ($-\mu_e\nabla^2 U_0$, where μ_e is the effective viscosity of porous medium) on the RHS of Eq. (1) and thus proposed a much more complicated formulation for the pressure loss through perforated plates, i.e. the so-called Brinkman-Forchheimer equation [52]. This equation is considered a more general description of the flow resistance in a porous medium because of the diffusion term (or Brinkman term) accounting for the boundary effect. However, this additional diffusion term is less significant for perforated plates [40] and is neglected in this study, as in many other previous studies [40,47,49].

3.1. The Bae & Kim model

Although Eq. (4) provides a mathematical description of the pressure loss through perforated plates, the permeability K and Forchheimer coefficient α are yet to be determined. On the basis of the numerical simulations of laminar flows ($Re_p < 25$), Bae & Kim [40] developed the following model to estimate K and α of the perforated plate.

$$K = \frac{\varepsilon D^2 \delta}{32\delta + 15 D}, \quad \alpha = \frac{3(1-\varepsilon)}{4\varepsilon^2 \delta}. \tag{5}$$

This model has been validated against the experiment of Doerffer & Bohning [53]. The reader may refer to Ref. [40] for the detailed comparison between the model predictions and the measurements.

To further assess the accuracy of the Bae & Kim model [40] in predicting turbulent flows through perforated plates, we apply the model to predict the recent experiment of Méry & Sebbane [38]. Fig. 2 shows
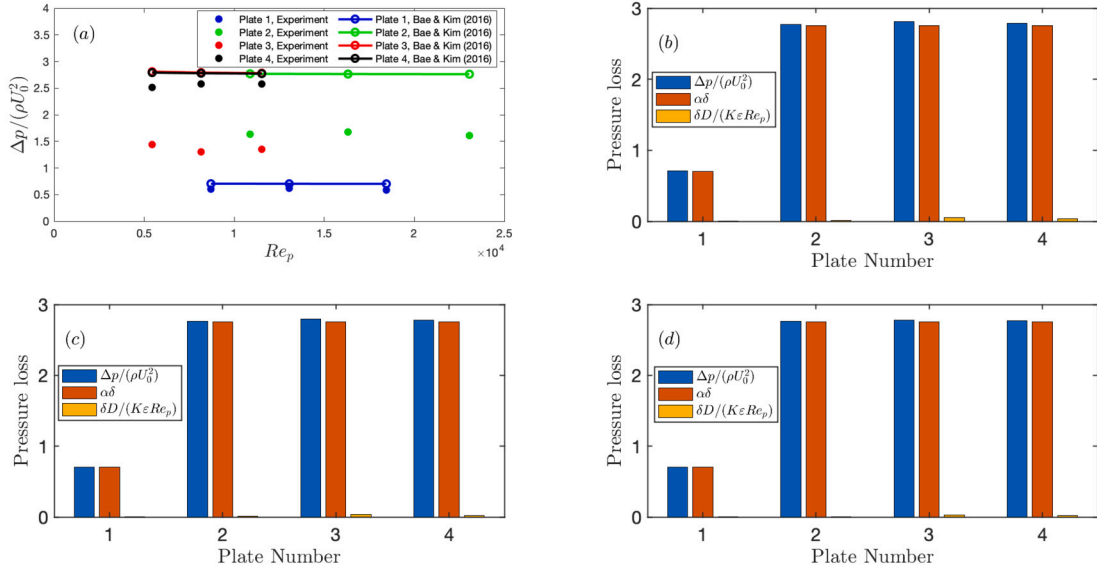
Fig. 2. (*a*) Comparison between the pressure loss ($\Delta p/(\rho U_0^2)$) predicted by the Bae & Kim model [40] and the experiment of Méry & Sebbane [38]; Comparison of the predicted pressure loss with its Forchheimer ($\alpha\delta$) and Darcy ($\delta D/(K\varepsilon Re_p)$) contributions at three different velocities: (*b*) 16.6 m/s; (*c*) 25 m/s; and (*d*) 35 m/s. (For interpretation of the colours in the figure(s), the reader is referred to the web version of this article.)
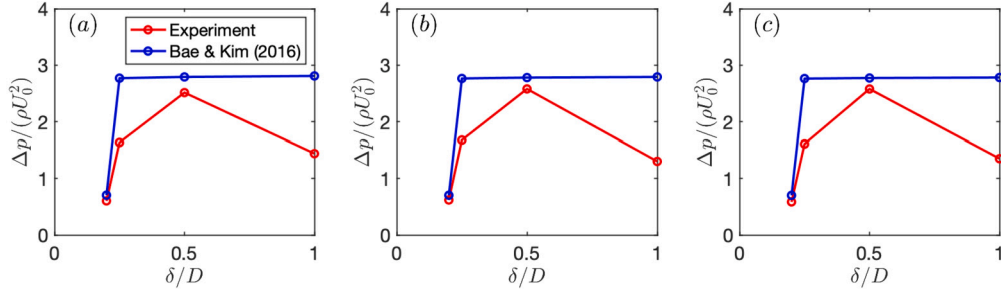

Fig. 3. Comparison of the pressure loss predicted by the Bae & Kim model [40] with the experiment of Méry & Sebbane [38] at three different flow velocities: (*a*) 16.6 m/s; (*b*) 25 m/s; and (*c*) 35 m/s.

a comparison of pressure drop between the prediction of the Bae & Kim model [40] and the experiment of Méry & Sebbane [38]. Although the predicted pressure drops of plates 1 and 4 are somewhat close to the experiment, those of plates 2 and 3 are not. It is also clear that the Darcy contribution, i.e. $\delta D/(K\varepsilon Re_p)$, is negligibly small and thus the Forchheimer contribution ($\alpha\delta$) dominates in the present turbulent flow regime. However, it is interesting to note that, at low Reynolds numbers ($Re_p < 25$), conversely, the Darcy contribution dominates over the Forchheimer contribution, as shown in Ref. [40]. In Fig. 2, the predicted pressure drops of plates 2, 3 and 4 (whose porosities are the same) are essentially similar due to the fact that the dominant Forchheimer contribution depends only on the plate porosity and not on the plate thickness ratio δ/D. Moreover, it is also found that both the experiment and the Bae & Kim model [40] show that the pressure drops are almost independent of the pore-level Reynolds number Re_p, again suggesting that the viscous Darcy contribution is negligibly small and the inertial Forchheimer contribution is dominant in the present flow regime. Overall, although the Bae & Kim model has been previously shown to perform very well in the prediction of laminar flows through perforated plates [40], its performance in turbulent flow predictions is not satisfying. Thus, an extension of the Bae & Kim model [40] to turbulent regimes is needed.

Fig. 3 shows a comparison of pressure drop between the prediction of the Bae & Kim model [40] and the experiment of Méry & Sebbane [38] at three different flow velocities. The predictions of plate 1 ($\delta/D = 0.2$) agree well with the experiments. For plates 2, 3 and 4 whose porosities are the same ($\varepsilon = 0.403$), the measured pressure drops vary with the plate thickness δ/D whereas the predicted ones do not. This is again because the dominant Forchheimer contribution of the Bae & Kim model [40] does not depend on the plate thickness ratio δ/D. Therefore, to extend the Bae & Kim model [40] to turbulent regimes, it is reasonable to propose a correction factor that takes into account the effect of plate thickness ratio.

3.2. An extension of the Bae & Kim model to turbulent regimes

Considering the differences between the experimental data and the prediction of the Bae & Kim model [40], a correction factor f, as a function of the plate porosity ε and thickness ratio δ/D, is proposed to correct the Forchheimer coefficient α so that the Bae & Kim model [40] becomes applicable for turbulent regimes while at the same time it remains effective in laminar regimes.

To propose a correction factor for the Forchheimer coefficient, quantitative analyses of the gaps between the predicted and measured pressure drops in Fig. 3 are needed. For plates 2, 3 and 4 whose porosities are the same ($\varepsilon = 0.403$), the measured pressure drops vary with the plate thickness δ/D like a parabola whereas the predicted ones are constant. Thus, to correct the predicted pressure drops of plates 2, 3 and 4, a parabolic-type multiplication factor is needed. Through fitting the experimental pressure drops of plates 2, 3 and 4 (whose porosities are constant, i.e. $\varepsilon = 0.403$), we propose a parabolic-type factor as $\left[6(\delta/D) - 5(\delta/D)^2\right]/2$. However, this additionally introduced factor will change the predicted pressure drop of plate 1 which was originally close to the experimental data. To remedy this, we need to propose

another multiplication factor that pulls the predicted pressure drop of plate 1 ($\varepsilon = 0.623$) back to the experimental data, and meanwhile does not change the already corrected pressure drops of plates 2, 3 and 4 ($\varepsilon = 0.403$). The factor $0.6/(1 - \varepsilon)$ is equal to 1 at $\varepsilon = 0.403$ and is equal to 1.6 at $\varepsilon = 0.623$, serving this purpose. By multiplying the aforementioned two factors, we finally construct a correction factor f for the Forchheimer coefficient, as follows

$$f\left(\varepsilon, \frac{\delta}{D}\right) = \frac{0.3}{1 - \varepsilon}\left[6\left(\frac{\delta}{D}\right) - 5\left(\frac{\delta}{D}\right)^2\right]. \qquad (6)$$

With the factor (Eq. (6)) to correct the Forchheimer coefficient, in the new model, the permeability and the Forchheimer coefficient become

$$K = \frac{\varepsilon D^2 \delta}{32\delta + 15D}, \quad \alpha = \frac{9}{40\varepsilon^2\delta}\left[6\left(\frac{\delta}{D}\right) - 5\left(\frac{\delta}{D}\right)^2\right]. \qquad (7)$$

Since the new model is obtained by proposing a correction factor (Eq. (6)) to the Forchheimer coefficient of the Bae & Kim model [40], it inherits some physical properties of the Bae & Kim model [40]. For example, the Forchheimer contribution dominates over the Darcy contribution in turbulent flow regimes whereas, at low Reynolds numbers, the Darcy contribution dominates over the Forchheimer contribution. Nevertheless, the present model also differs from the Bae & Kim model [40] in that its Forchheimer contribution varies with plate thickness (δ/D). This is likely due to different flow patterns within the length of the pores. The flow through a perforated plate usually features flow separation near the leading edge of the pores. On the one hand, the separated flow inside the pores reattaches within the length of the pores if the plate is thick enough, resulting in a closed recirculation zone. On the other hand, the separated flow inside the pores does not reattach within the length of the pores if the plate is too thin, resulting in an unclosed recirculation region and a much more chaotic wake downstream of the plate [39]. The different flow patterns within the length of the pores and in the downstream of the plates play an important role in affecting the pressure loss. The validation of this proposed model is presented in Section 4.1 for laminar flows and in Section 4.2 for turbulent flows.

4. Results

In this section, we validate the proposed model (Eq. (7)) against existing numerical simulations in laminar regimes and experiments in turbulent regimes. We also compare our new model with other previous models [33,42–44] (see Appendix).

4.1. Laminar flow

Shahzad et al. [49] performed numerical simulations to study the pressure losses of laminar flows through perforated plates. Here, the numerical simulations of three perforated plates are deployed to validate the proposed model. They have the same plate thickness ratio $\delta/D = 0.25$ and different porosities $\varepsilon = 0.2$, 0.4 and 0.5. Fig. 4 shows a comparison of the pressure drops predicted by both the present model (Eq. (7)) and the Bae & Kim model [40] with the numerical simulations. Since the correction factor $f(\varepsilon, \delta/D)$ is less than 1 for these perforated plates, the present model gives smaller predictions of pressure drops than the Bae & Kim model [40] does. This is more obvious for the plate with $\varepsilon = 0.2$ since the correction factor decreases with a decrease of plate porosity. It is also interesting to note that, the agreement between the present model and the Bae & Kim model [40] is better at $\varepsilon = 0.4$ and 0.5 than at $\varepsilon = 0.2$, probably because the porosities of the perforated plates used to design the correction factor (Eq. (6)) are between 0.4 and 0.63 and the perforated plate here with $\varepsilon = 0.2$ is relatively far away from this porosity range. In other words, the present model probably has better prediction capabilities for plates with a moderate porosity that is not far away from the range between 0.4 and 0.63. Overall, compared with the numerical simulations of Shahzad et al.
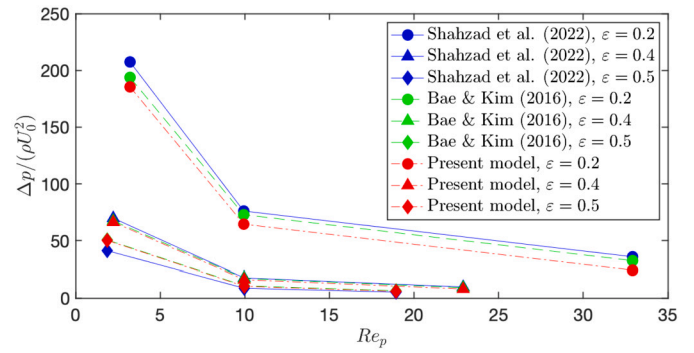

Fig. 4. Comparison of the pressure drops predicted by the present model (Eq. (7)) and the Bae & Kim model [40] with the numerical simulations of Shahzad et al. [49].
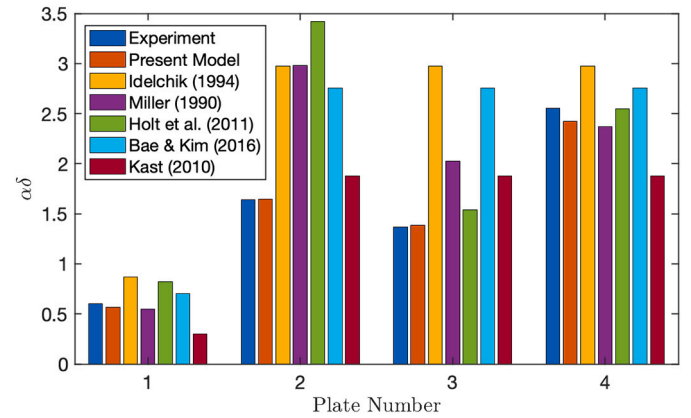

Fig. 5. Comparison of the Forchheimer part of the pressure drop predicted by the present model with the measured pressure drops of Méry & Sebbane [38] and the predictions by other previous models [33,42–44]. Note that the pressure-drop values of the experiment are the average of the three values associated with the three different flow speeds for each plate.

[49], both models give reasonable predictions of the pressure drops, demonstrating the capability of both models in predicting laminar flows through perforated plates. In fact, since at low Reynolds numbers the Darcy contribution of pressure drop dominates over the Forchheimer contribution, the present model inherits the prediction capability from the Bae & Kim model [40].

4.2. Turbulent flow

Since the correction factor (Eq. (6)) was proposed on account of the differences between the experimental data of Méry & Sebbane [38] and the prediction of the Bae & Kim model [40], we first validate the proposed model against the experimental data set of Méry & Sebbane [38] in turbulent regimes. Fig. 5 shows a comparison of the Forchheimer part of the predicted pressure drop with the experiment of Méry & Sebbane [38] and the predictions by other previous models [33,42–44]. The Forchheimer part basically represents the total pressure drop, since in turbulent regimes the Forchheimer contribution strongly dominates over the Darcy contribution, as shown in Fig. 2. According to Fig. 5, with the correction factor in Eq. (6), it is evident that the present model gives an excellent agreement with the experiment and performs better than other previous models do. This observation is further underscored by the comparison of the prediction errors of different pressure-drop models with respect to the experiment of Méry & Sebbane [38], as shown in Fig. 6. However, it should be noted that the present comparisons with the experiment of Méry & Sebbane [38] are not completely convincing to validate the new model since the proposed correction factor was based on the same set of experimental data. It is thus more con-
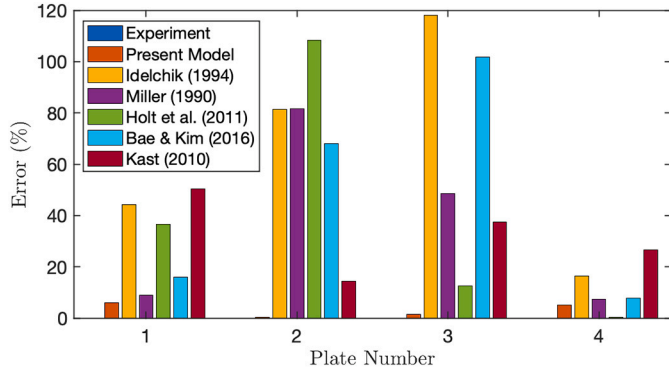
Fig. 6. Comparison of the prediction errors of different pressure-drop models with respect to the experiment of Méry & Sebbane [38]. The legend is the same as that of Fig. 5.
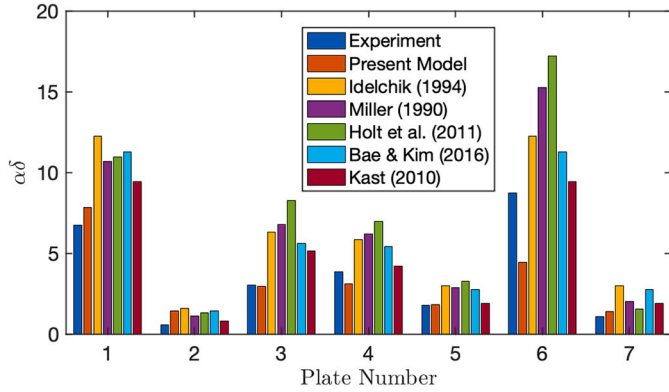

Fig. 7. Comparison of the Forchheimer part of the pressure drop predicted by the present model with the measured pressure drops of Yuvuzkurt & Catchen [37] and the predictions by other previous models [33,42–44]. In this figure, for plate 3, the results have been multiplied by 0.1 in order to have a better scale of the plot. Note also that the pressure-drop values of the experiment are the average of all values associated with different pore-level Reynolds numbers for each plate.

vincing to demonstrate the prediction capability of the present model by validating the present model against another independent set of experimental data.

Fig. 7 shows a comparison of the Forchheimer part of the pressure drop predicted by the present model with the experiment of Yuvuzkurt & Catchen [37] and the predictions by other previous models [33,42–44]. On the one hand, compared with the experiment, the present model gives reasonable predictions with relatively small discrepancies for plates 1, 3, 4, 5 and 7. Nevertheless, an obvious discrepancy is observed for plate 6, due to the fact that (i) the thickness ratio of plate 6 is at the endpoint of the thickness ratio range between 0.2 and 1.0 and (ii) the porosity of plate 6 is relatively far away from the porosity range between 0.4 and 0.63 (see Table 3). It is also observed that plates 1, 3 and 4 with porosities lower than the aforementioned porosity range give relatively good predictions. This suggests that, as long as the plate thickness ratio is relatively far larger than the lower endpoint of the aforementioned thickness ratio range, the plate porosity does not necessarily need to fall exactly into the porosity range between 0.4 and 0.63 in order for the present model to produce good predictions. In other words, the plate thickness ratio plays a relatively more important role than the porosity does in the present model. On the other hand, compared with other previous models [33,42–44], Figs. 7 and 8 suggest that the present model overall produces better agreement with the experiment of Yuvuzkurt & Catchen [37] than other models do. This is significant, considering that the present model is in a much simpler form than the models of Idelchik [42], Miller [33], Holt et al. [44] and
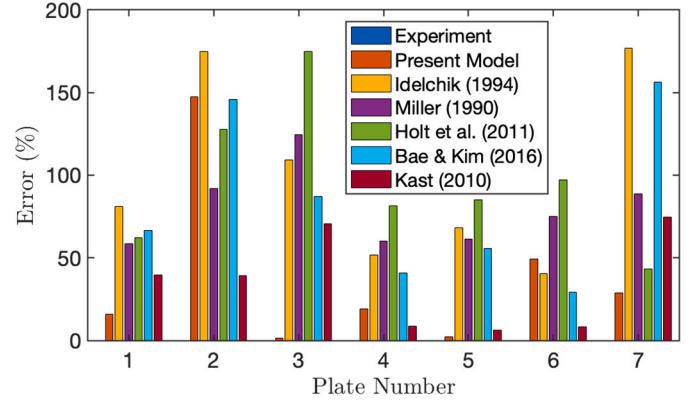

Fig. 8. Comparison of the prediction errors of different pressure-drop models with respect to the experiment of Yuvuzkurt & Catchen [37]. The legend is the same as that of Fig. 7.

Kast [43] (see Appendix). Interestingly, it is also observed in Fig. 7 that the measured pressure drop of plate 2 is rather small, likely due to the large openness of the plate. Consequently, although the absolute discrepancies between the experiment and the various models look small, the relative errors shown in Fig. 8 are not small. Besides, it is noted that the error of a specific model can approximate 200% in Fig. 8. This highlights the formidable challenge of precisely modeling pressure loss in the complex problem of flow-through perforated plates.

5. Application of the present model in numerical simulations

5.1. Numerical modelling of perforated plates in two-dimensional channel flows

For perforated plates consisting of very fine pores, the direct meshing of the perforated plates is very challenging since it would result in a large number of computational cells. In such cases, a numerical model to represent the effects of flow-through perforated plates is favoured. Similar to the modelling of other porous medium [50,54–56], the effect of perforated plates in flows can be modelled by adding a pressure-drop source term to the momentum equations. Within the perforated-plate region, a volume source term S is added to the right-hand side (RHS) of the momentum equations, yielding the RANS momentum equations as [57]

$$\frac{\partial(\rho\bar{u}_i)}{\partial t} + \frac{\partial(\rho\bar{u}_i\bar{u}_j)}{\partial x_j} = -\frac{\partial\bar{p}}{\partial x_i} + \frac{\partial\bar{\sigma}_{ij}}{\partial x_j} + \frac{\partial\sigma_{ij,RANS}}{\partial x_j} + S_i, \tag{8}$$

where $\bar{u}_i$ is the components of velocity (for two-dimensional flows, $i =1$, 2), $\bar{p}$ is the pressure, $\bar{\sigma}_{ij}$ is the viscous stress tensor and $\sigma_{ij,RANS}$ is the Reynolds-stress tensor. Outside the perforated-plate region, the governing equations are the original Navier-Stokes equations (i.e. without the additional source term S_i in Eq. (8)). In the whole flow domain (including the perforated-plate region), the continuity equation is also the original one due to the fact that the law of mass conservation is still satisfied in the porous region, as follows

$$\frac{\partial\rho}{\partial t} + \frac{\partial(\rho\bar{u}_i)}{\partial x_i} = 0. \tag{9}$$

If the two-dimensional air flow approaches the perforated plate at zero incident angle, the source term is expressed as

$$\begin{bmatrix} S_1 \\ S_2 \end{bmatrix} = \begin{bmatrix} -\mu\bar{u}/K - \rho\alpha\,|\bar{u}|\,\bar{u} \\ 0 \end{bmatrix}, \tag{10}$$

where $\bar{u}$ is the streamwise velocity. The parameters K and α are given by the present model in Eq. (7). Since the incoming flow direction is perpendicular to the perforated plate, the second component of the source term S_2 is zero.

Inlet   Outlet

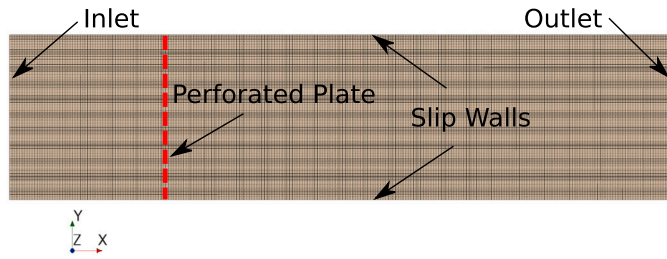Perforated Plate

Slip Walls

Fig. 9. The two-dimensional coarse mesh with a cell size of $\Delta = 0.5$ mm for the numerical simulations. The dashed line indicates the location where the source term is applied in the momentum equations.

5.2. Computational meshes and simulation set-up

The computational domain is a rectangle of 200×50 mm^2. Three different computational meshes consisting of square cells of different sizes are deployed in the simulations. The coarse mesh has a cell size of $\Delta = 0.5$ mm, while the medium and fine meshes have a cell size of $\Delta = 0.25$ and 0.125 mm, respectively. The cell numbers of the coarse, medium and fine meshes are 40k, 160k and 640k, respectively. Fig. 9 shows the coarse computational mesh. The perforated plate is not meshed, whereas its effect is modelled by adding a momentum source (see Eq. (10)) at the location of the dashed line ($x = 0$). More specifically, for plates 1, 2 and 4 with a thickness of 1 mm, the momentum source is applied to the cells within -0.5 mm $< x < 0.5$ mm. For plate 3 with a thickness of 2 mm, the momentum source is applied to the cells within -1 mm $< x < 1$ mm.

We perform steady RANS simulations with the SST k-ω model using the commercial Siemens STAR-CCM+ version 2021.1 [58]. The inlet velocity is $U_0 = 16.6$ m/s, leading to a Reynolds number of $Re = 27370$ based on the inlet velocity and the channel half height. At the inlet boundary, the turbulence intensity is 6.2% and the turbulent viscosity ratio is 10.0, which gives the dissipation rate ω.

5.3. Pressure drop predicted by RANS simulations with the present model as a momentum source

Fig. 10 shows the pressure drops predicted by RANS simulations. The convergence of the solutions using the medium and fine meshes is well demonstrated. However, the coarse mesh ($\Delta = 0.5$ mm) seems to be too coarse for accurately predicting the pressure drops of plates 1, 2 and 4. Meanwhile, it is also observed that the coarse mesh ($\Delta = 0.5$ mm) gives a fairly good prediction for plate 3. To understand the reason, for plates 1, 2 and 4, we perform additional simulations using the same coarse mesh but with the source term applied to the cells within -1 mm $< x < 1$ mm instead of -0.5 mm $< x < 0.5$ mm, reducing the pressure drop in each cell by 50% in order to keep the overall resistance the same. As such, all four plates are represented by 4 cells in the streamwise direction because the cell size is $\Delta = 0.5$ mm. Fig. 11 shows the simulation results. It is clear that the solutions using 4 cells in the streamwise direction to represent the perforated plates converge to the solutions of the medium mesh ($\Delta = 0.25$ mm). This suggests that, when modelling perforated plates (and probably also other porous plates), the modelling thickness of the plate, whether the same as the physical thickness of the plate or not, is less important. Rather, the number of cells used to represent the plate is more important [50]. It is suggested to have at least 4 cells in the streamwise direction to represent the flow through perforated plates.

The RANS-predicted pressure drops are also listed in Table 4 for a comparison with the measured pressure drops and the model-predicted pressure drops. The results pertaining to the simulations on the medium mesh using 8 cells in the streamwise direction to represent the perforated plates are also listed in the table. Overall, the RANS predictions agree very well with the present model predictions. Note that we also
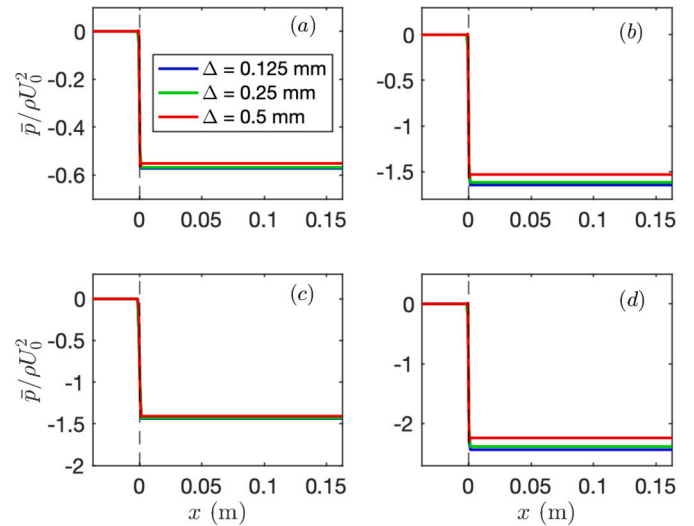

Fig. 10. The RANS-predicted pressure drops using the coarse, medium and fine meshes. (*a*) Plate 1; (*b*) Plate 2; (*c*) Plate 3; and (*d*) Plate 4. The vertical black dashed line indicates the location ($x = 0$) where the source term is applied in the momentum equations. From (*a*) to (*d*), the percentage differences of the predicted pressure drop between the medium and fine meshes are 0.66%, 1.76%, 0.42% and 2.17%, respectively.
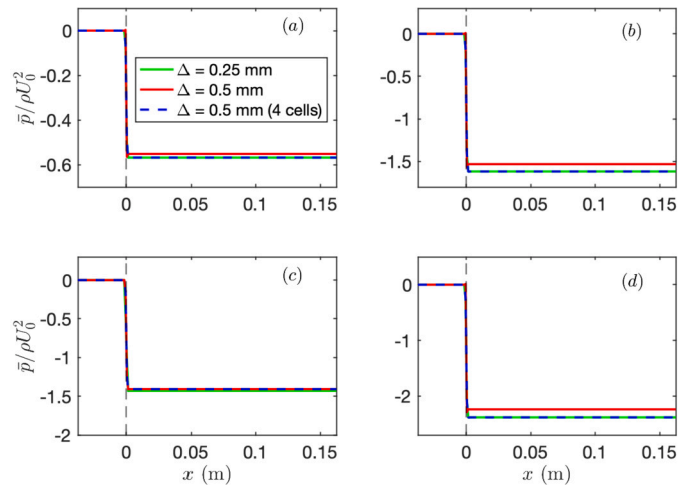

Fig. 11. The RANS-predicted pressure drops using the coarse and medium meshes. For the coarse mesh, simulations are also performed using 4 cells in the streamwise direction to represent the perforated plate. (*a*) Plate 1; (*b*) Plate 2; (*c*) Plate 3; and (*d*) Plate 4. The vertical black dashed line indicates the location ($x = 0$) where the source term is applied in the momentum equations.

Table 4
Comparison between the measured pressure drops ($\Delta p/(\rho U_0^2)$) of Méry & Sebbane [38] and the pressure drops predicted by the present perforated-plate model and by numerical simulations using the medium mesh.

Plate	1	2	3	4
Experiment	0.605	1.635	1.440	2.515
Present model	0.574	1.658	1.438	2.459
RANS Prediction	0.568	1.618	1.430	2.384
RANS Prediction[a]	0.572	1.647	1.430	2.436

[a] There are 8 cells in the streamwise direction for all 4 plates.

perform inviscid flow simulations. The results are the same as the RANS simulations. For brevity, the results associated with the inviscid flow simulations are not shown here.

6. Concluding remarks

A fluid flow through a perforated plate is a common problem in a wide variety of practical applications in thermal, mechanical, chemical, civil, nuclear, ocean and aerospace engineering [59]. In this paper, we proposed a novel fluid flow model for pressure loss through perforated plates in both laminar and turbulent flows. The design of this model is based on the recent experimental data of Méry & Sebbane [38], as well as the existing model of Bae & Kim [40] for laminar flows. The data used for the model design is a new experimental data set because the data has not been used to study the pressure-loss formulation of perforated plates, although the experiment itself has recently been published in Méry & Sebbane [38].

The pressure losses caused by flow-through perforated plates are often characterized by the Darcy-Forchheimer equation. The Darcy term corresponds to the viscous pressure loss while the Forchheimer term represents the inertial pressure loss. It has been shown by Bae & Kim [40] that, at low Reynolds numbers ($Re_p < 25$), the Darcy contribution to the normalized pressure drop dominates over the Forchheimer contribution. In turbulent regimes, however, it is found that the Forchheimer contribution strongly dominates. Moreover, the existing model of Bae & Kim [40] was only applicable to laminar flows. For these reasons, we proposed a correction to the Forchheimer coefficient of the Bae & Kim model [40] to enable the modelling of perforated plates in both laminar and turbulent flows. The new model is then validated against existing numerical simulations in the laminar regime and experiments in the turbulent regime. Overall, the predictions given by the new model agree well with the numerical simulations and experiments, and are superior to other models in the literature [33,42–44]. The proposed model is novel in that it has better accuracy in pressure-loss prediction than other existing models, compared to two independent sets of experimental measurements. Besides, the model has a very wide applicable range of Reynolds numbers, ranging from very-low-Reynolds-number laminar to very-high-Reynolds-number turbulent flows. Moreover, it is much simpler than the models of Idelchik [42], Miller [33], Holt et al. [44] and Kast [43] (see Appendix).

To demonstrate the new model's applicability in numerical simulations, two-dimensional channel flows are simulated using RANS with the new model as a pressure-drop source term added to the momentum equations. Overall, the RANS predictions agree very well with the present model predictions. In the numerical simulations, it is suggested to have at least 4 cells in the streamwise direction to represent the flow-through perforated plates.

Although the present model is applicable for a wide range of Reynolds numbers ranging from laminar to turbulent regimes, the limitation of the model is that the new model is only applicable for a certain range of plate porosities (ε) and plate thickness ratios (δ/D). This is limited by the experimental data used for the design of the present model. On the one hand, the model is applicable to a plate thickness ratio of $0.2 < \delta/D < 1$ because the correction factor f would go negative as $\delta/D > 1.2$. On the other hand, the present model probably has good prediction capabilities for plates with a moderate porosity that is not far away from the range between 0.4 and 0.63. The authors suggest an applicable porosity range between 0.3 and 0.7. Fortunately, these ranges of plate porosities and thicknesses have enabled the use of perforated plates in numerous engineering problems, e.g. heat transfer in heat exchangers, flame control in combustion chambers, aerodynamic noise abatement, etc. Pressure loss occurs due to energy dissipation as the flow expands from the vena contracta, where local velocity reaches its maximum. Thus, the location of the vena contracta significantly influences pressure loss. However, this pivotal location is subject to variation influenced by plate porosity and thickness ratio. The present model

may encounter limitations at porosities and thickness ratios beyond the aforementioned ranges, possibly stemming from inaccurate predictions of the location of the vena contracta under these conditions. In addition, limited by the absence of experimental data on perforated plates featuring various perforation shapes like triangles, rectangles, polygons, etc., it remains uncertain whether the current model's applicability extends to perforated plates with alternative geometries, although some studies indicate that pressure loss might be independent of perforation geometry [47].

CRediT authorship contribution statement

Shuai Li: Writing – review & editing, Writing – original draft, Visualization, Validation, Software, Methodology, Investigation, Formal analysis, Data curation, Conceptualization. **Lars Davidson:** Writing – review & editing, Visualization, Supervision, Funding acquisition, Formal analysis. **Shia-Hui Peng:** Writing – review & editing, Funding acquisition.

Declaration of competing interest

The authors declare that they have no known competing financial interests or personal relationships that could have appeared to influence the work reported in this paper.

Data availability

Data will be made available on request.

Appendix A. Empirical formulae for the pressure loss through perforated plates

Besides the aforementioned model of Bae & Kim [40] which was designed using numerical simulations of laminar flows, here we append some other popular models (formulae) for estimating the Forchheimer coefficient α. These formulae were proposed in experimental studies at high Reynolds numbers where the Forchheimer term strongly dominates over the Darcy term. Thus, the Forchheimer coefficient α can be used to calculate the Forchheimer contribution which is approximately equal to the pressure loss.

For perforated plates of finite thickness at high Reynolds numbers, Idelchik [42] proposed a formula of the form

$$\alpha = \frac{1}{2\varepsilon^2\delta}\left(0.5 + 0.24\sqrt{1-\varepsilon}(1-\varepsilon) + (1-\varepsilon)^2\right). \tag{11}$$

Similarly, Kast [43] suggested the following formula

$$\alpha = \frac{1}{2\varepsilon^2\delta}\left(\left(\frac{1}{C}-1\right)^2 + (1-\varepsilon)^2\right), \tag{12}$$

where C is a coefficient depending upon the plate porosity and can be expressed as

$$C = 0.6 + 0.4\varepsilon^2. \tag{13}$$

Miller [33] proposed the following formula

$$\alpha = C_0 \frac{(1 - C_c \varepsilon)^2}{2C_c^2 \varepsilon^2 \delta}, \tag{14}$$

where C_0 is a coefficient that depends on δ/D, and C_c is the jet contraction coefficient that depends on ε. According to Fratino [60], C_0 can be calculated by the following empirical expression, valid for $0.1 < \delta/D < 3$,

$$C_0 = 0.5 + \frac{0.178}{4(\frac{\delta}{D})^2 + 0.355}, \tag{15}$$

while C_c is given by

$$C_c = 0.596 + 0.0031 \exp(\frac{\sqrt{\varepsilon}}{0.206}). \tag{16}$$

Holt et al. [44] proposed a piecewise function for the Forchheimer coefficient, as follows

$$\alpha = \begin{cases} \frac{1}{2\delta}\left(2.9 - 3.79\frac{\delta}{D}\varepsilon^{0.2} + 1.79\left(\frac{\delta}{D}\right)^2 \varepsilon^{0.4}\right) K_{LA} & \frac{\delta}{D}\varepsilon^{0.2} < 0.9 \\ \frac{1}{2\delta}\left(0.876 + 0.069\frac{\delta}{D}\varepsilon^{0.2}\right) K_{LA} & \frac{\delta}{D}\varepsilon^{0.2} > 0.9, \end{cases} \tag{17}$$

where the jet contraction coefficient C_c is set to be 0.72 [46]. K_{LA} is the pressure loss coefficient of a single-hole orifice as estimated by a theoretical model for reattached flows, as follows

$$K_{LA} = 1 - \frac{2}{\varepsilon} + \frac{2}{\varepsilon^2}\left(1 - \frac{1}{C_c} + \frac{1}{2C_c^2}\right). \tag{18}$$

References

[1] Y. Ahmimache, M. Fénot, F. Plourde, L. Descamps, Heat transfer and flow velocity study of a row of jets emerging from a perforated pipe at a low Reynolds number, Int. J. Heat Mass Transf. 183 (2022) 122067.

[2] D.H. Lee, Y.M. Lee, Y.T. Kim, S.Y. Won, Y.S. Chung, Heat transfer enhancement by the perforated plate installed between an impinging jet and the target plate, Int. J. Heat Mass Transf. 45 (1) (2002) 213–217.

[3] H. McMahon, R. Bowen, G. Bleyle Jr, A perforated-plate heat exchanger, Trans. Am. Soc. Mech. Eng. 72 (5) (1950) 623–632.

[4] S. Shevyakova, V. Orlov, Study of hydraulic resistance and heat transfer in perforated-plate heat exchangers, Inzh.-Fiz. Zh. 45 (1) (1983) 32–36.

[5] C.F. Kutscher, Heat exchange effectiveness and pressure drop for air flow through perforated plates with and without crosswind, J. Heat Transf. 116 (2) (1994) 391–399.

[6] M. White, G. Nellis, S. Klein, W. Zhu, Y. Gianchandani, An experimentally validated numerical modeling technique for perforated plate heat exchangers, J. Heat Transf. 132 (11) (2010).

[7] M. Tomić, P. Živković, M. Vukić, S. Ayed, The methodology for determination of perforated plate heat transfer coefficient, in: International Conference Powerplants, 2014.

[8] V.K. Arghode, Y. Joshi, Experimental investigation of air flow through a perforated tile in a raised floor data center, J. Electron. Packag. 137 (1) (2015).

[9] L.R. Raju, S.S. Kumar, K. Chowdhury, T. Nandi, Heat Transfer and Flow Friction Correlations for Perforated Plate Matrix Heat Exchangers, IOP Conference Series: Materials Science and Engineering, vol. 171, IOP Publishing, 2017, p. 012085.

[10] M.A. Tomić, S.K. Ayed, Ž.Ž. Stevanović, P.S. Ðekić, P.M. Živković, M.V. Vukić, Perforated plate convective heat transfer analysis, Int. J. Therm. Sci. 124 (2018) 300–306.

[11] H. Husin, M. Faisal, A. Gani, R. Sardjono, R. Mamat, The modification of the perforated plate in the fluidized-bed combustor to analyze heat convection rate and temperature, J. Combust. 2021 (2021) 1–8.

[12] E. Laws, A. Ouazzane, A further investigation into flow conditioner design yielding compact installations for orifice plate flow metering, Flow Meas. Instrum. 6 (3) (1995) 187–199.

[13] E. Spearman, J. Sattary, M. Reader-Harris, Comparison of velocity and turbulence profiles downstream of perforated plate flow conditioners, Flow Meas. Instrum. 7 (3–4) (1996) 181–199.

[14] B. Laribi, P. Wauters, M. Aichouni, Comparative study of aerodynamic behaviour of three flow conditioners, Eur. J. Mech. Environ. Eng. 48 (1) (2003) 21–30.

[15] W. Xiong, K. Kalkühler, W. Merzkirch, Velocity and turbulence measurements downstream of flow conditioners, Flow Meas. Instrum. 14 (6) (2003) 249–260.

[16] J. Hoffmann-Vocke, J. Neale, M. Walmsley, The effect of inlet conditions on the air side hydraulic resistance and flow maldistribution in industrial air heaters, Int. J. Heat Fluid Flow 32 (4) (2011) 834–845.

[17] W. Yaïci, M. Ghorab, E. Entchev, 3d cfd analysis of the effect of inlet air flow maldistribution on the fluid flow and heat transfer performances of plate-fin-and-tube laminar heat exchangers, Int. J. Heat Mass Transf. 74 (2014) 490–500.

[18] B. Laribi, A.A. Hadj, Discharge coefficient behaviour in presence of four perforated plates flow conditioners-numerical investigation part 1, in: 17th International Congress of Metrology, EDP Sciences, 2015, p. 03005.

[19] N. Noiray, D. Durox, T. Schuller, S. Candel, Passive control of combustion instabilities involving premixed flames anchored on perforated plates, Proc. Combust. Inst. 31 (1) (2007) 1283–1290.

[20] S. Oh, Y. Shin, Y. Kim, Stabilization effects of perforated plates on the combustion instability in a lean premixed combustor, Appl. Therm. Eng. 107 (2016) 508–515.

[21] S.S. Rashwan, A.H. Ibrahim, T.W. Abou-Arab, M.A. Nemitallah, M.A. Habib, Experimental study of atmospheric partially premixed oxy-combustion flames anchored over a perforated plate burner, Energy 122 (2017) 159–167.

[22] J. Kim, A. Satija, R.P. Lucht, J.P. Gore, Effects of turbulent flow regime on perforated plate stabilized piloted lean premixed flames, Combust. Flame 211 (2020) 158–172.

[23] H. Younesian, M. Shahmardan, Experimental study of flame quenching phenomenon of mixed methane and air in the presence of perforated plates and porous barriers in a closed chamber, Fuel Combust. 14 (2) (2021) 87–100.

[24] H. Younesian, M. Nazari, M.M. Shahmardan, Visualization of flame propagation and quenching of methane/air mixture in a cubic enclosure with perforated plates: experimental study, Combust. Sci. Technol. (2022) 1–20.

[25] D. Naot, F. Kreith, On the penetration of turbulence through perforated flat plates, Int. J. Heat Mass Transf. 23 (4) (1980) 566–568.

[26] R. Liu, D.S. Ting, G.W. Rankin, On the generation of turbulence with a perforated plate, Exp. Therm. Fluid Sci. 28 (4) (2004) 307–316.

[27] R. Liu, D.S.-K. Ting, Turbulent flow downstream of a perforated plate: sharp-edged orifice versus finite-thickness holes, J. Fluids Eng. 129 (9) (2007) 1164–1171.

[28] S. Dhineshkumar, B. Prakash, S. Balakrishnan, Large turbulence creation inside a gas turbine combustion chamber using perforated plate, Int. J. Eng. Sci. Res. Technol. 2 (2013) 937–942.

[29] K. Sakaliyski, J. Hileman, Z. Spakovszky, Aero-acoustics of perforated drag plates for quiet transport aircraft, in: 45th AIAA Aerospace Sciences Meeting and Exhibit, 2007, p. 1032.

[30] A. Rubio Carpio, F. Avallone, D. Ragni, M. Snellen, S. Van Der Zwaag, Mechanisms of broadband noise generation on metal foam edges, Phys. Fluids 31 (10) (2019) 105110.

[31] P. Laffay, S. Moreau, M.C. Jacob, J. Regnard, Experimental investigation of the noise radiated by a ducted air flow discharge though diaphragms and perforated plates, J. Sound Vib. 472 (2020) 115177.

[32] C. Sumesh, T. Jothi, Aerodynamic noise from an asymmetric airfoil with perforated extension plates at the trailing edge, Int. J. Aeroacoust. 20 (1–2) (2021) 88–108.

[33] D.S. Miller, Internal Flow Systems, vol. 5, BHRA (Information Services), Bedford, UK, 1990.

[34] J.C. Pacio, C.A. Dorao, A study of the effect of flow maldistribution on heat transfer performance in evaporators, Nucl. Eng. Des. 240 (11) (2010) 3868–3877.

[35] K.K. Nielsen, K. Engelbrecht, C.R. Bahl, The influence of flow maldistribution on the performance of inhomogeneous parallel plate heat exchangers, Int. J. Heat Mass Transf. 60 (2013) 432–439.

[36] L. Beckedorff, R. Da Silva, G. Martins, K. de Paiva, J. Oliveira, A. Oliveira, Flow maldistribution and heat transfer characteristics in plate and shell heat exchangers, Int. J. Heat Mass Transf. 195 (2022) 123182.

[37] S. Yavuzkurt, G.L. Catchen, Dependence of pressure losses on angle of attack for flow through perforated plates, in: ASME International Mechanical Engineering Congress and Exposition, vol. 37165, 2003, pp. 435–440.

[38] F. Méry, D. Sebbane, Aerodynamic characterisation of porous fairings: pressure drop and laser Doppler velocimetry measurements, Sci. Data 10 (1) (2023) 39.

[39] Y. Bayazit, E.M. Sparrow, D.D. Joseph, Perforated plates for fluid management: plate geometry effects and flow regimes, Int. J. Therm. Sci. 85 (2014) 104–111.

[40] Y. Bae, Y.I. Kim, Numerical modeling of anisotropic drag for a perforated plate with cylindrical holes, Chem. Eng. Sci. 149 (2016) 78–87.

[41] I.E. Idelchik, Handbook of Hydraulic Resistance, Washington, 1986.

[42] I.E. Idelchik, Handbook of Hydraulic Resistance, 2nd edn, CRC, Boca Raton, FL, 1994.

[43] W. Kast, Pressure drop in single phase flow, in: VDI Heat Atlas, 2010.

[44] G. Holt, D. Maynes, J. Blotter, Cavitation at sharp edge multi-hole baffle plates, in: ASME International Mechanical Engineering Congress and Exposition, vol. 54921, 2011, pp. 401–410.

[45] Engineering Sciences Data Unit (ESDU), Flow of liquids. Pressure losses across orifice plates, perforated plates and thick orifice plates in ducts, Tech. Rep., Internal Flow and Physical Properties Group, London, UK, 1981, Report no. 81039.

[46] S. Malavasi, G. Messa, U. Fratino, A. Pagano, On the pressure losses through perforated plates, Flow Meas. Instrum. 28 (2012) 57–66.

[47] P. Tanner, J. Gorman, E. Sparrow, Flow–pressure drop characteristics of perforated plates, Int. J. Numer. Methods Heat Fluid Flow 29 (11) (2019) 4310–4333.

[48] A. Minotti, F. Simon, F. Gantié, Characterization of an acoustic liner by means of laser Doppler velocimetry in a subsonic flow, Aerosp. Sci. Technol. 12 (5) (2008) 398–407.

[49] H. Shahzad, S. Hickel, D. Modesti, Permeability and turbulence over perforated plates, Flow Turbul. Combust. 109 (4) (2022) 1241–1254.

[50] S. Li, L. Davidson, S.-H. Peng, Numerical modeling of a wire mesh for aerodynamic noise reduction, Phys. Fluids 35 (1) (2023) 015103.

[51] S. Lee, J. Yang, Modeling of Darcy-Forchheimer drag for fluid flow across a bank of circular cylinders, Int. J. Heat Mass Transf. 40 (13) (1997) 3149–3155.

[52] K. Vafai, C.L. Tien, Boundary and inertia effects on flow and heat transfer in porous media, Int. J. Heat Mass Transf. 24 (2) (1981) 195–203.

[53] P.P. Doerffer, R. Bohning, Modelling of perforated plate aerodynamics performance, Aerosp. Sci. Technol. 4 (8) (2000) 525–534.

[54] P.N. Okolo, K. Zhao, J. Kennedy, G.J. Bennett, Numerical modeling of wire screens for flow and noise control, in: 23rd AIAA/CEAS Aeroacoustics Conference, 2017, p. 3700.

[55] W. Zhu, Z. Xiao, S. Fu, Numerical modeling screen for flow and noise control around tandem cylinders, AIAA J. 58 (6) (2020) 2504–2516.

[56] M. Terracol, E. Manoha, Numerical wire mesh model for the simulation of noise-reduction devices, AIAA J. 59 (3) (2021) 987–1007.

[57] Siemens Digital Industries Software, Simcenter STAR-CCM+ User Guide v. 2021.1, Siemens, 2021.

[58] Siemens Digital Industries Software, Simcenter STAR-CCM+, version 2021.1, Siemens, 2021.

[59] S. Li, L. Davidson, S.-H. Peng, A fluid flow model for the pressure loss through perforated plates, arXiv preprint, arXiv:2304.11730, 2023.

[60] U. Fratino, Hydraulic and cavitation characteristics of multihole orifices, in: Proceedings of the Hydraulic Machinery and System 20th IAHR Symposium, 2000, pp. 6–9.